Spectral methods and the ECMWF model

Atmosphere and Ocean Dynamics, Lecture 7: notes

Pedro S. Peixoto

December 2, 2026

Abstract

Spectral methods represent every field by global waves: Fourier series on a periodic interval, spherical harmonics on the sphere. These notes discuss the spectral derivative and its accuracy, products and aliasing (the transform method and the 2/3 rule), the barotropic vorticity equation on the sphere, semi-implicit time steps, the ECMWF model (IFS) and the cost of its transforms, the spectral models in use today, and the spectral method as a Galerkin method.

Table of contents

1 Two limits of grid methods 2

2 Von Neumann's trick (1950) 3

3 Global or local? 4

4 Spectral derivative (1/3): interpolate 5

5 Spectral derivative (2/3): differentiate 6

6 Spectral derivative (3/3): all waves exact 6

7 How fast does the error fall? 7

8 Advection without numerical dispersion 8

9 Derivatives, advection and aliasing, computed 8

10 A few waves do the work of many grid points 9

11 Products (1/3): two waves make new waves 9

12 Products (2/3): the transform method 10

13 Products (3/3): aliasing 11

14 The 2/3 rule 12

15 In class: aliasing on a small grid 12

16 What the exercise showed 13

17 From the plane to the sphere 13

18 On the sphere (1/3): the Poisson problem 14

19 On the sphere (2/3): to the grid and back 15

20 On the sphere (3/3): one time step 16

21 Triangular truncation and the Gaussian grid 17

22 In class: Rossby–Haurwitz waves 18

23 What the exercise showed 19

24 The barotropic vorticity equation, computed on a plane and on the sphere 19

25 Model against exact solutions: Rossby waves, a drifting cyclone, an unstable jet 20

26 Semi-implicit (1/2): the gravity-wave limit 21

27 Semi-implicit (2/2): Helmholtz, a division 21

28 The grids of the IFS 22

29 IFS today 23

30 The cost of the transforms 24

31 Spectral models today 25

32 A Galerkin method 26

33 Key points 27

Further reading 27

References 27

1 Two limits of grid methods

Grid-point methods have two limits (Figure 1). Applied to the advection of a wave $e^{i(kx-\omega t)}$, the centred difference gives $\omega = c\sin(k\Delta x)/\Delta x$, a phase speed $c^* = \omega/k = c\sin(k\Delta x)/(k\Delta x) < c$: short waves move too slowly, and on M points the wave $k = M/2$, of wavelength $2\Delta x$, does not move at all; a narrow hump leaves a trail of wiggles behind it (numerical dispersion). On the sphere the CFL condition becomes the **pole problem**: on a latitude–longitude grid the meridians meet at the poles, and with a spacing of 1° the east–west distance between points is 111 km at the equator, 19 km at 80°N and 1 km on the row next to the pole (at 89.5°N, with the points at the centres of the cells). The CFL condition there forces a time step a hundred times shorter than at the equator, unless the short waves near the poles are filtered (Williamson 2007; Durran 2010, Sect. 3.3, 6.4.2). Can a derivative be exact for every wave the grid carries, and can a global model avoid the tiny steps of the poles?

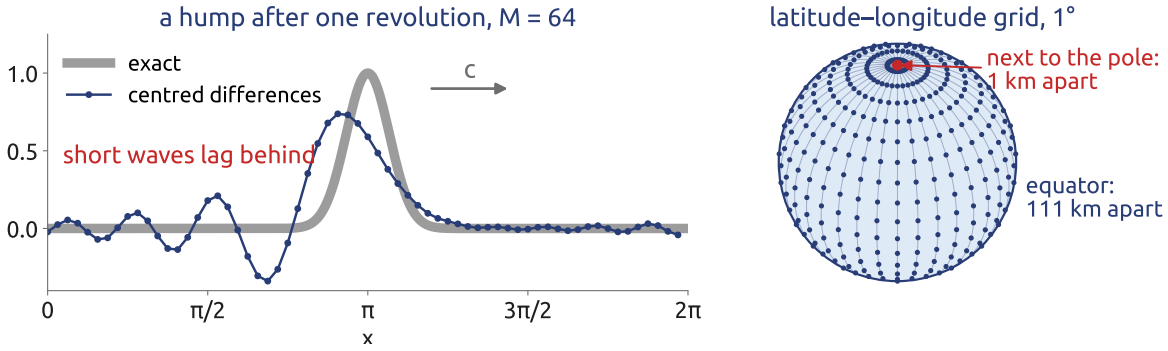


Figure 1: Left: the advection equation $u_t + c\,u_x = 0$ with a narrow Gaussian hump, $u_0 = e^{-((x-\pi)/0.3)^2}$, carried once around a periodic domain of length 2π on 64 points, with the centred second-order difference and RK4 at Courant number 0.1 (so the error is that of the space derivative): the short waves lag behind. Right: a latitude–longitude grid (drawn every 10°) seen from above 35°N; with a 1° spacing, neighbouring points are 111 km apart at the equator and 1 km apart next to the pole, at 89.5°N.

2 Von Neumann's trick (1950)

The ENIAC forecast of Charney et al. (1950) was a finite-difference model, and a regional one. The barotropic vorticity equation for the 500 hPa height was written on a polar stereographic map, a plane tangent at the North Pole; the curvature of the Earth then enters only through the map factor $m = 2/(1+\sin\varphi)$, with $\nabla^2_{\text{globe}} = m^2\nabla^2_{\text{map}}$ and $J_{\text{globe}} = m^2 J_{\text{map}}$, so that the operators are those of a flat plane. The domain was a rectangle over North America of 19 by 16 grid points ($P = 18$ by $Q = 15$ intervals Δs, 736 km at the pole and 494 km at 20°N), with centred differences in space and a leapfrog step in time (Lynch 2008, appendix A). A regional domain needs boundary conditions: Charney, Fjørtoft and von Neumann showed that the height on the whole boundary, and the vorticity where the flow enters, determine the motion, and the boundary heights were held fixed through each 24-hour forecast.

At every step the Jacobian gave the tendency of the vorticity, and the tendency of the height (here written with the streamfunction, $\psi = gz/f_0$ in Lynch's re-creation) followed from a Poisson problem, zero on the boundary:

$$(\delta_x^2 + \delta_y^2)\,\partial_t\psi = -J(\psi, \zeta + f), \qquad \delta_x^2 f_i = \frac{f_{i+1} - 2f_i + f_{i-1}}{\Delta s^2},$$

with the 5-point Laplacian $\delta_x^2 + \delta_y^2$ built from centred second differences (notation of Durran 2010, Sect. 3.1) and the map factor on the right-hand side. Platzman (1979, 310) tells that, of the arithmetic done by the ENIAC, "the only nontrivial ones were the four in which the Laplacian was inverted to solve Poisson's equation". Von Neumann solved it with a direct method. With zero boundary values, the discrete sines are the eigenvectors of the 5-point Laplacian: from $\sin(a+b) + \sin(a-b) = 2\sin a\cos b$,

$$\delta_x^2 \sin\frac{p\pi i}{P} = \frac{2\cos(p\pi/P) - 2}{\Delta s^2}\,\sin\frac{p\pi i}{P} = -\frac{4}{\Delta s^2}\sin^2\frac{p\pi}{2P}\,\sin\frac{p\pi i}{P},$$

and likewise in y, so that

$$(\delta_x^2 + \delta_y^2)\Big[\sin\frac{p\pi i}{P}\,\sin\frac{q\pi j}{Q}\Big] = -\frac{4}{\Delta s^2}\Big[\sin^2\frac{p\pi}{2P} + \sin^2\frac{q\pi}{2Q}\Big]\,\sin\frac{p\pi i}{P}\,\sin\frac{q\pi j}{Q},$$

for $p = 1, \ldots, P-1$ and $q = 1, \ldots, Q-1$. Expanding the right-hand side in these sines (a sine transform in x, then one in y), dividing each coefficient by its eigenvalue, and summing back

(two more sine sums) gives the tendency: the four transforms of each step, Platzman's operations 5, 8, 11 and 13. In his words, it is "one of a class of direct methods in which an exact solution of the discrete problem is obtained in a finite number of steps", chosen because of the peculiar limitations of the ENIAC (Platzman 1979, 310; Lynch 2008, appendix A).

So the 1950 forecast was not a spectral model: the derivatives, the Jacobian included, were finite differences, and the sines only inverted the discrete Laplacian. The eigenvalue is the square of the modified wavenumber of the centred difference, $(2/\Delta s)\sin(p\pi/2P)$: for long waves it tends to the eigenvalue of the exact Laplacian on the rectangle, $-[(p\pi/L_x)^2 + (q\pi/L_y)^2]$ with $L_x = P\Delta s$, $L_y = Q\Delta s$, and it is smaller for short ones. Spectral methods go further: they represent *every* field, and every derivative, by a sum of eigenfunctions of the exact Laplacian: on a periodic interval the Fourier waves, on the sphere the spherical harmonics. The first model of that kind was Silberman's, in 1954 (Silberman 1954).

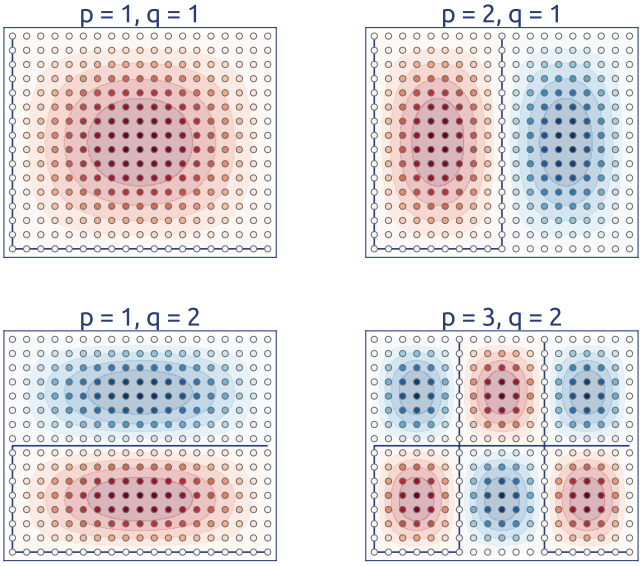


Figure 2: Four discrete sines $\sin(p\pi i/P)\sin(q\pi j/Q)$, eigenvectors of the 5-point Laplacian on the rectangle of the 1950 forecast (19 by 16 grid points, 736 km apart at the pole of the polar stereographic map): dots at the grid points, coloured by their value (red positive, blue negative), over the continuous sine whose samples they are (faint); the navy lines are its zeros. Each one is only multiplied by a number when the 5-point Laplacian acts on it.

3 Global or local?

A finite-difference scheme approximates a derivative at a point from a few neighbours: it fits a local polynomial. A spectral method writes the whole field as a sum of global functions. On a periodic interval of length 2π,

$$u(x) = \sum_k \hat{u}_k \, e^{ikx},$$

and every wave e^{ikx} spans the whole domain (Figure 3). A change of u at one point changes every coefficient; the derivative at one point depends on the values at all points. This makes spectral methods very accurate for smooth fields, and also explains their cost and their trouble with discontinuities (Durran 2010, Sect. 6.2; Fornberg 1996).

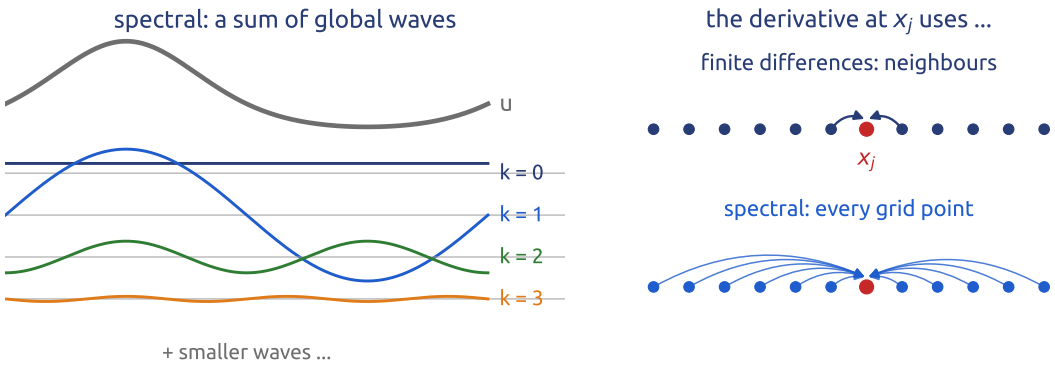


Figure 3: Left: the field $e^{\sin x} - 1$ and its first waves, from the FFT. Right: the derivative at a grid point uses two neighbours (centred difference) or every grid point (spectral).

4 Spectral derivative (1/3): interpolate

Throughout, M is the number of grid points and N the largest wavenumber kept (the truncation). On M equally spaced points $x_j = j\Delta x$, $\Delta x = 2\pi/M$, $j = 0, \ldots, M-1$, the M values u_j and M coefficients $\hat{u}_k$ are related by the **discrete Fourier transform**

$$\hat{u}_k = \frac{1}{M} \sum_{j=0}^{M-1} u_j \, e^{-ikx_j}, \qquad u_j = \sum_{k=-M/2+1}^{M/2} \hat{u}_k \, e^{ikx_j} \qquad (M \text{ even}).$$

The second formula follows from the first by the discrete orthogonality $\frac{1}{M}\sum_j e^{i(k-l)x_j} = 1$ if $k - l$ is a multiple of M, and 0 otherwise. Evaluated for any x (with the wave $k = M/2$ taken as $\hat{u}_{M/2}\cos(Mx/2)$, since on the grid it is $(-1)^j$), the sum is a smooth periodic function that passes through every grid value: the *trigonometric interpolant* (Figure 4). The fast Fourier transform computes the M coefficients in $O(M \log M)$ operations instead of M^2 (Durran 2010, Sect. 6.2; Fornberg 1996). (numpy's `fft` returns $M\hat{u}_k$.)

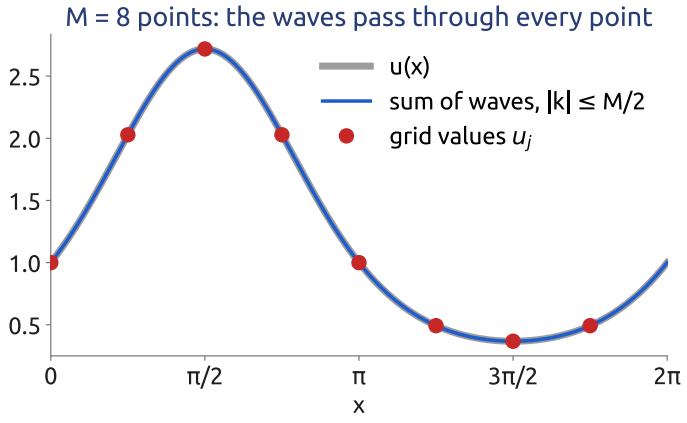


Figure 4: Eight grid values and the sum of waves $|k| \le M/2$ through them: the trigonometric interpolant passes through every grid point.

5 Spectral derivative (2/3): differentiate

Differentiating the interpolant term by term,

$$\left(\frac{\partial u}{\partial x}\right)_j = \sum_k ik\,\hat{u}_k\, e^{ikx_j},$$

so the derivative is three steps: FFT, multiply each coefficient by ik, inverse FFT (Figure 5). Each wave is shifted by a quarter wavelength and multiplied by k. The wave $k = M/2$ is $\cos(Mx_j/2) = (-1)^j$ on the grid; the derivative of $\cos(Mx/2)$ vanishes at the grid points, so its coefficient is set to zero (for the second derivative, $-k^2$, it can be kept). In spectral space, ∂_x is a multiplication by ik and ∇^2 by $-k^2$ (Durran 2010, Sect. 6.2).

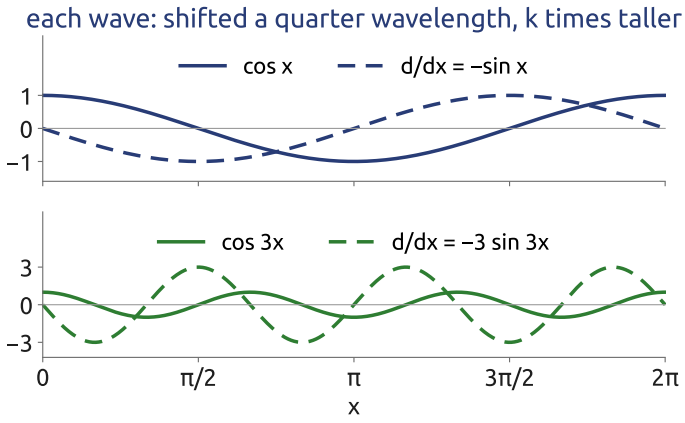


Figure 5: The derivative of two waves: each is shifted by a quarter wavelength and multiplied by its wavenumber k ($\cos x \to -\sin x$, $\cos 3x \to -3\sin 3x$).

6 Spectral derivative (3/3): all waves exact

Apply a derivative approximation to a single wave $u = e^{ikx}$ in the advection equation $u_t + c\,u_x = 0$. The centred second-order difference gives

$$\frac{e^{ik(x+\Delta x)} - e^{ik(x-\Delta x)}}{2\Delta x} = i\,\frac{\sin k\Delta x}{\Delta x}\,e^{ikx}, \qquad \omega = \frac{c\,\sin k\Delta x}{\Delta x}, \qquad \frac{c^*}{c} = \frac{\sin k\Delta x}{k\Delta x}$$

(Durran 2010, Sect. 3.3.1), with the numerical phase speed $c^* = \omega/k$; the fourth-order difference gives $c^*/c = (8\sin k\Delta x - \sin 2k\Delta x)/(6k\Delta x)$. Both are close to 1 for long waves ($k\Delta x \ll 1$) and fall below it for short ones; the $2\Delta x$ wave ($k\Delta x = \pi$) has $c^* = 0$. The spectral derivative has $c^* = c$ for every $|k| < M/2$: it is exact for every wave the grid can carry (Figure 7, Figure 6).

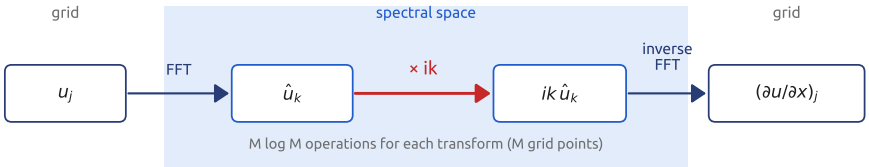


Figure 6: The spectral derivative: FFT to the wave coefficients, a multiplication by ik, inverse FFT back to the grid.

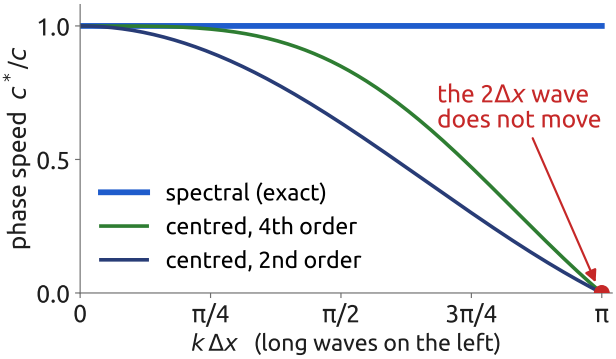


Figure 7: Numerical phase speed c^*/c of three approximations of ∂_x in the advection equation (wave e^{ikx}), against $k\Delta x$: the centred differences of second and fourth order fall below 1 for short waves, and give zero for the $2\Delta x$ wave; the spectral derivative is exact up to $k\Delta x = \pi$.

7 How fast does the error fall?

For the smooth function $u = e^{\sin x}$, the largest error of $\partial_x u$ with $M = 32$ points is 2.6×10^{-2} for the centred second-order difference, 1.1×10^{-3} for the fourth-order one, and 2.9×10^{-15} (round-off) for the spectral derivative. The error of a scheme of order p falls like M^{-p}; the spectral error falls faster than any power of M (Figure 8). A square wave, with jumps, rings (the Gibbs phenomenon) and converges slowly everywhere.

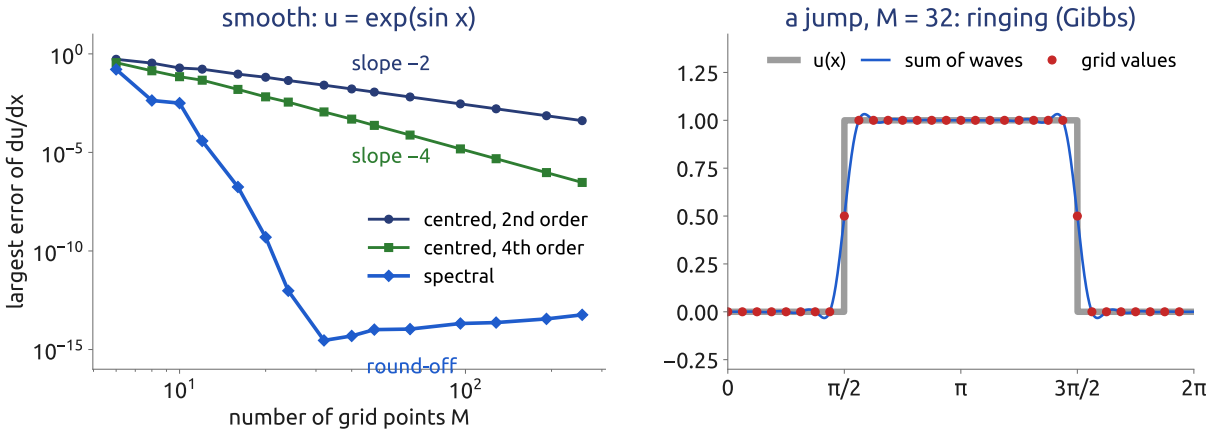


Figure 8: Left: largest error of $\partial_x u$ for $u = e^{\sin x}$ against the number of points M, for centred differences of order 2 and 4 (slopes -2 and -4) and the spectral derivative, which reaches round-off near $M = 32$. Right: a square wave on 32 points and the sum of its waves through the grid values, which overshoots near the jumps (Gibbs).

Mathematical aside: why. If u is periodic and p times continuously differentiable, integrating by parts p times gives $|\hat{u}_k| \le C/|k|^p$. If u is analytic in a strip $|\mathrm{Im}\, x| < \alpha$ of the complex plane, $|\hat{u}_k| \le Ce^{-\alpha|k|}$. The coefficients $\tilde{u}_k$ computed from the grid values (the discrete Fourier transform) are the exact ones $\hat{u}_k$ plus their aliases,

$$\tilde{u}_k = \sum_{r=-\infty}^{\infty} \hat{u}_{k+rM}$$

(this follows from the discrete orthogonality), so the interpolant misses only the waves beyond

$M/2$ and their aliases, both of size about $e^{-\alpha M/2}$, and the error of the derivative is of order $Me^{-\alpha M/2}$: exponential convergence, "spectral accuracy" (Fornberg 1996; Durran 2010, Sect. 6.2.1). A function with a jump has $|\hat{u}_k| \sim 1/|k|$: the interpolant oscillates near the jump and converges slowly, and because the waves are global the error is felt everywhere. Fronts, cloud edges, coastlines and steep orography are the hard cases for spectral models.

8 Advection without numerical dispersion

For the advection equation $\partial_t u + c\,\partial_x u = 0$, the spectral method gives one ordinary differential equation per wave,

$$\frac{d\hat{u}_k}{dt} = -ick\,\hat{u}_k, \qquad \hat{u}_k(t) = \hat{u}_k(0)\,e^{-ickt}\,:$$

every resolved wave moves at exactly c, and there is no numerical dispersion in space; only the time stepping adds errors. With a centred difference the wave k moves at $c^* = c\sin(k\Delta x)/(k\Delta x) < c$: the short waves that make up a narrow hump lag behind it and leave a trail of wiggles (Figure 9). Williamson (2007) notes this as one of the reasons spectral models dominated from the late 1970s: "linear advection is accurate to the truncation limit". The weather, though, is nonlinear: $\mathbf{u}\cdot\nabla\zeta$ is a product.

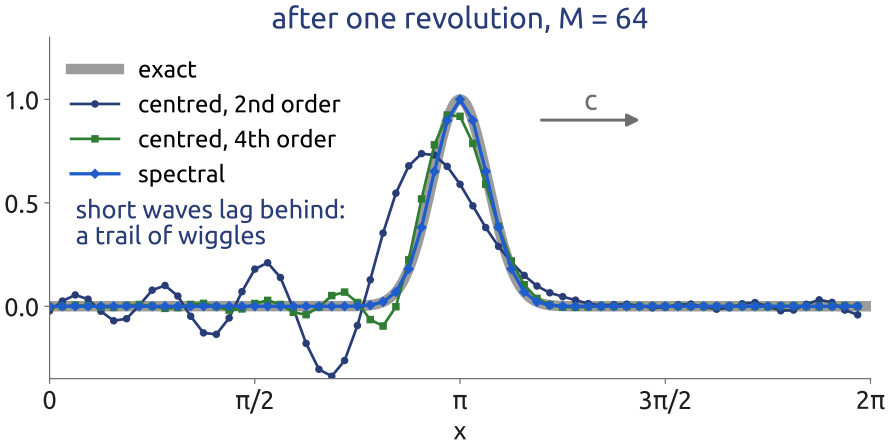


Figure 9: A narrow hump advected once around a periodic domain of 64 points with RK4 and a small time step (Courant number 0.1): centred differences of order 2 and 4 leave a trail of wiggles behind the hump; the spectral solution lies on the exact one (gray).

9 Derivatives, advection and aliasing, computed

A few lines of numpy (an FFT, a multiplication by ik, an inverse FFT) are enough to measure these properties: how fast the coefficients of a smooth field, a field with a kink and one with a jump fall; the error of the spectral derivative against the centred differences of order 2 and 4, whose slopes -2 and -4 follow from their order; the advection of a hump for 1 and 10 revolutions, and the largest stable time step; and, once products are introduced, aliasing in u^2 on a small grid and Burgers' equation with and without the 2/3 rule (Figure 10).

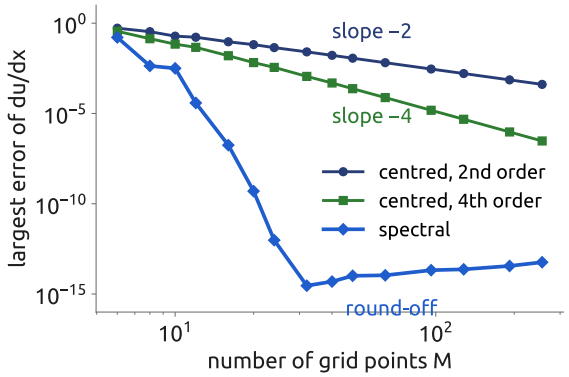


Figure 10: The error of the three derivatives against the number of points M: slopes -2 and -4 for the centred differences, and the spectral drop to round-off.

10 A few waves do the work of many grid points

The errors of $\partial_x u$ for $u = e^{\sin x}$ with $M = 32$ are 2.6×10^{-2} (centred, second order), 1.1×10^{-3} (fourth order) and 2.9×10^{-15} (spectral). After 10 revolutions of the hump the errors are 0.65, 0.36 and 6×10^{-5} (Figure 11). The price is a shorter time step. The fastest spectral wave has frequency $|\omega| = c\,k_{\max} \approx c\pi/\Delta x$, against $c/\Delta x$ for the centred difference. With RK4, stable for $|\omega|\Delta t \le 2\sqrt{2}$, the spectral method needs a Courant number $c\Delta t/\Delta x \lesssim 2\sqrt{2}/\pi \approx 0.9$, the centred difference $\lesssim 2.8$: the shortest waves move at full speed. For smooth fields, a few waves do the work of many grid points. A kink ($|\sin x|$) makes the spectral error away from the kink only about $1/M$: a defect spreads over the whole domain.

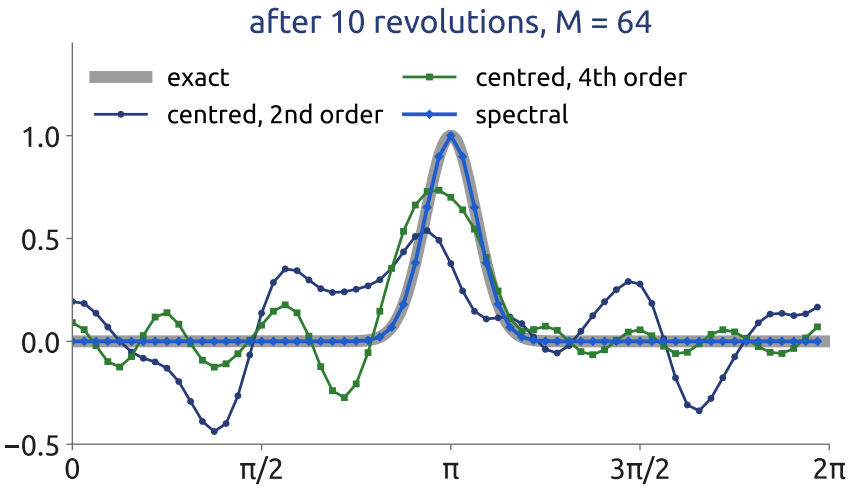


Figure 11: The hump after 10 revolutions: the centred schemes have lost it in their wiggles, the spectral one keeps it.

11 Products (1/3): two waves make new waves

The equations are nonlinear: $u\,\partial_x u$, $\mathbf{u} \cdot \nabla\zeta$. A product of two waves is $e^{ikx}e^{ilx} = e^{i(k+l)x}$; for example $\cos 3x \cos 4x = \frac{1}{2}\cos x + \frac{1}{2}\cos 7x$: sum and difference waves (Figure 12). If $u = \sum_l \hat{u}_l e^{ilx}$

and $v = \sum_l \hat{v}_l e^{ilx}$ contain the waves $|l| \le N$, every pair of waves l and $k-l$ makes the wave k:

$$u\,v = \sum_k \Big(\sum_l \hat{u}_l\, \hat{v}_{k-l} \Big)\, e^{ikx}, \qquad \widehat{(uv)}_k = \sum_l \hat{u}_l\, \hat{v}_{k-l},$$

so the product contains waves up to $|k| = 2N$, and in spectral space it is a convolution, which costs $O(N^2)$ operations per product in one dimension, and much more on the sphere, where the interaction coefficients of spherical harmonics must be stored. Silberman (1954) integrated the barotropic vorticity equation in spherical harmonics in this way, the first spectral model in meteorology (Ehrendorfer 2012, Sect. 7.3); Robert (1966) did the same for the primitive equations, at very low resolution. The cost kept spectral models small until 1970.

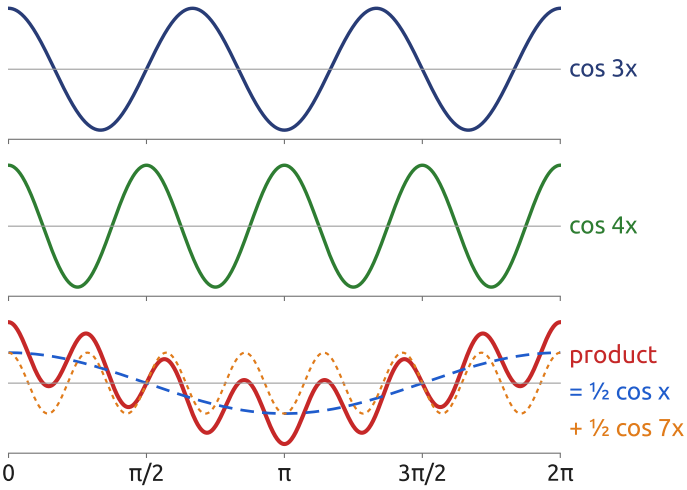


Figure 12: $\cos 3x$, $\cos 4x$ and their product, the sum of $\frac{1}{2}\cos x$ and $\frac{1}{2}\cos 7x$.

12 Products (2/3): the transform method

The transform method (Orszag 1970; Eliasen et al. 1970): compute the product on the grid. From the coefficients of u and of $\partial_x v$, two inverse FFTs give their grid values; multiply them point by point (M operations); one FFT gives the coefficients of the product. The cost is $O(M \log M)$. Derivatives and other linear operators are applied in spectral space, products on the grid: the *pseudo-spectral* or *spectral transform* method (Durran 2010, Sects. 6.2.2 and 6.3) (Figure 13). It made spectral models cost-effective, and from the mid to late 1970s it dominated global weather and climate modelling (Williamson 2007). (Names differ between books: Durran (2010) calls *pseudospectral* the collocation version, with as many grid points as waves, which aliases, and keeps *spectral* for the version with enough grid points to remove aliasing; Ehrendorfer (2012, Sect. 7.7) and the weather-prediction literature speak of the *spectral transform method* in both cases.) The product has waves up to $2N$, with N the truncation, but a grid of M points carries only the waves $|k| \le M/2$: where do the others go?

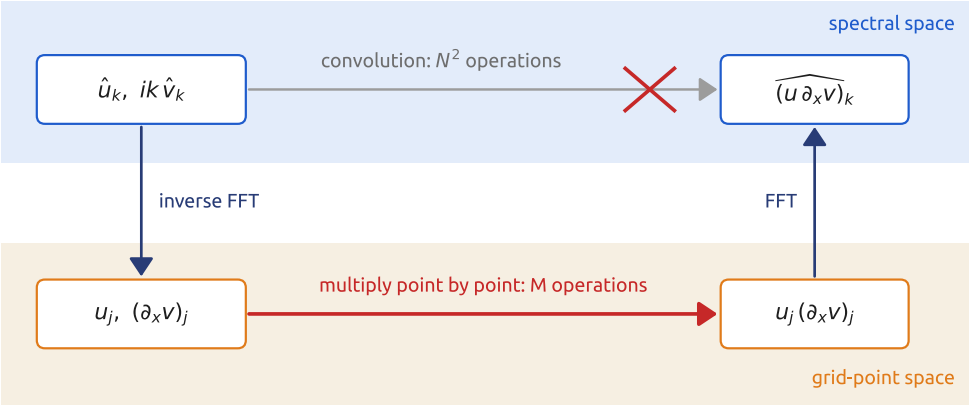


Figure 13: The transform method for a product $u\,\partial_x v$. In spectral space the product is a convolution, with N^2 operations (crossed out); instead, two inverse FFTs bring the factors to the grid, they are multiplied point by point (M operations) and one FFT brings the product back.

13 Products (3/3): aliasing

On a grid of M points, $e^{i(k+M)x_j} = e^{ikx_j}e^{iMx_j} = e^{ikx_j}$, because $Mx_j = 2\pi j$. The waves k and $k \pm M$ take the same values at every grid point: the grid cannot tell them apart, and a wave too short for the grid is seen as a longer one, its *alias* (Figure 14). On 8 points, for example, $\cos 6x_j = \cos(6-8)x_j = \cos 2x_j$. In terms of coefficients: if $u(x) = \sum_k \hat{u}_k e^{ikx}$ exactly, the coefficients computed from the M grid values are

$$\tilde{u}_k = \frac{1}{M}\sum_{j=0}^{M-1} u_j\, e^{-ikx_j} = \sum_{r=-\infty}^{\infty} \hat{u}_{k+rM},$$

by the discrete orthogonality: each computed coefficient is the exact one plus the exact coefficients of all its aliases. For $u = \cos 6x$ ($\hat{u}_{\pm 6} = \frac{1}{2}$) on 8 points, $\tilde{u}_{\pm 2} = \frac{1}{2}$ and $\tilde{u}_{\pm 6}$ does not exist: the grid sees $\cos 2x$. When a product is computed on the grid, its waves beyond the grid's range come back as aliases on the kept waves: wrong energy at small scales. In a nonlinear model this can grow without bound: the *nonlinear instability* found by Phillips in 1959 in a finite-difference model (Durran 2010, Sect. 4.5, 6.3; Ehrendorfer 2012, Sect. 7.9–7.10).

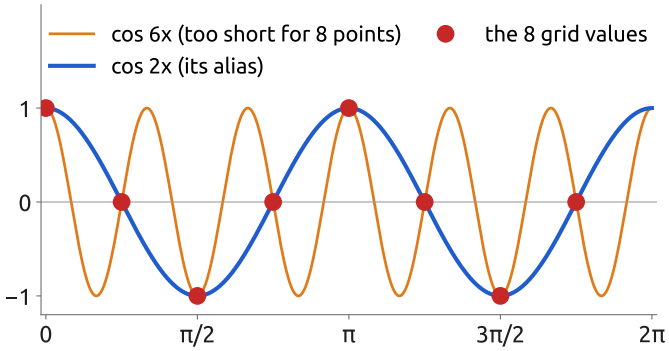


Figure 14: The wave $\cos 6x$, too short for 8 grid points, and $\cos 2x$, its alias: they take the same values at the grid points.

14 The 2/3 rule

Suppose u and v keep the waves $|k| \le N$ and the product is computed on M points. The product has waves up to $2N$; the wave $2N$ is seen as $2N - M$. To keep every alias away from the kept waves we need $2N - M < -N$, that is

$$M \ge 3N + 1.$$

The waves of the product between N and $M/2$ are represented on the grid and simply dropped by the truncation; those beyond $M/2$ alias onto $k \le -N - 1$ and are dropped too. So with three grid points per shortest kept wave the kept coefficients of a quadratic product are exact. Equivalently, on a given grid of M points one keeps only the waves $|k| < M/3$, the lower two thirds: the "2/3 rule" (Orszag 1971; Durran 2010, Sect. 6.3). For T42 this gives $3 \cdot 42 + 1 = 127$, and the T42 grid has 128 longitudes (Figure 15). The IFS names its grids by the number of points per shortest wave: linear (2), quadratic (3), cubic (4).

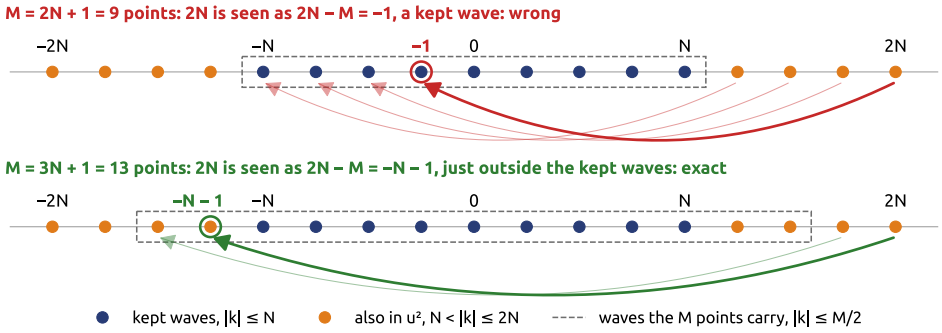


Figure 15: Why three points per shortest wave, drawn for $N = 4$. Navy dots: the kept waves $|k| \le N$; orange dots: the other waves of u^2, $N < |k| \le 2N$; dashed box: the waves the M grid points carry, $|k| \le M/2$. A wave k beyond the box is seen as $k - M$ (arrows; the negative side folds the same way); the bold arrow follows the largest wave, $2N$, to $2N - M$. Top: $M = 2N + 1$, and $2N$ lands on -1, a kept wave. Bottom: $M = 3N + 1$, and $2N$ lands on $-N - 1$, the first wave outside the kept ones: every alias falls on a discarded wave

15 In class: aliasing on a small grid

Exercise 1 — Aliasing on a small grid. Take the $M = 8$ grid points $x_j = 2\pi j/8$. (a) Show that $\cos 6x_j = \cos 2x_j$ at every grid point. Which waves look like $k = 1$ on this grid? (b) $u = \cos 3x$ is carried by the grid. What does the grid see for $u^2 = \frac{1}{2} + \frac{1}{2}\cos 6x$? (c) A field keeps the waves $|k| \le N$. How many points M are needed so that no alias of u^2 falls on a kept wave? Check T42 and its 128 longitudes.

(d) To hand in: cubic products. The same question for u^3. Which fraction of the grid's waves can be kept? ECMWF's model uses a "cubic" grid, with four points per shortest wave: why the name?

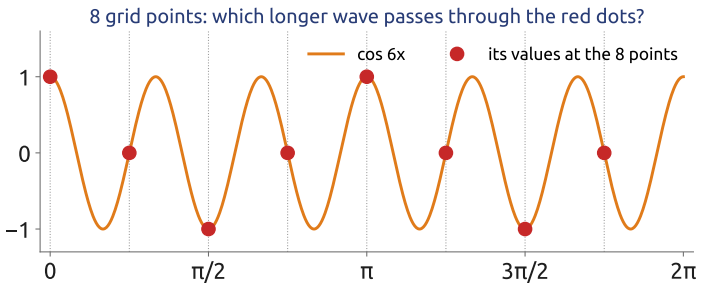


Figure 16: The wave $\cos 6x$ and its values at the 8 grid points $x_j = 2\pi j/8$.

16 What the exercise showed

(a) On 8 points k and $k \pm 8$ agree: $\cos 6x_j = \cos(-2x_j) = \cos 2x_j$, and $k = 1$ looks like $9, -7, 17, \ldots$ (b) $u^2 = \frac{1}{2} + \frac{1}{2}\cos 6x$ is seen as $\frac{1}{2} + \frac{1}{2}\cos 2x$: a wave that is not in u^2 at all. (c) The alias of $2N$ is $2N - M$, which must be below $-N$: $M \geq 3N + 1$; T42: $127 \leq 128$ longitudes. (d) u^3 has waves up to $3N$, so $M \geq 4N + 1$: keep half of the grid's waves; the "cubic" grid of the ECMWF model, with four points per shortest wave, computes cubic products without aliasing on the kept waves. A check with a random field of waves $|k| \leq 10$ (Figure 17): the error of the kept coefficients drops to round-off at $M = 31$ for u^2 and $M = 41$ for u^3.

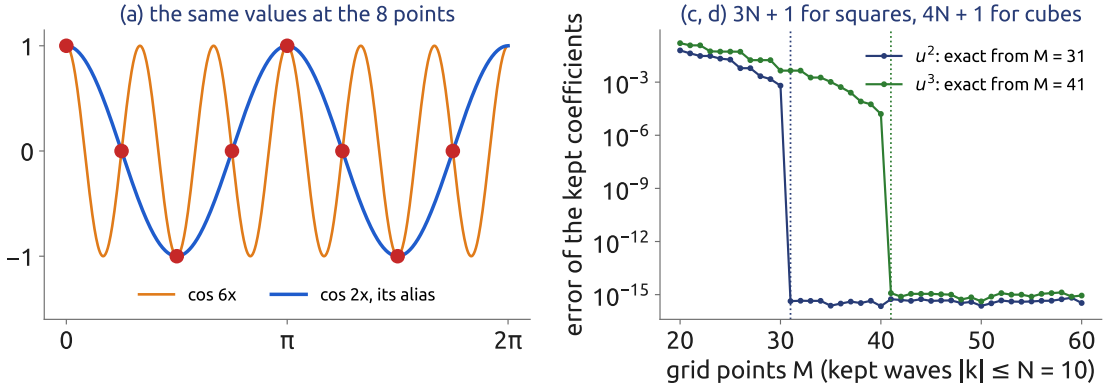


Figure 17: Left: $\cos 6x$ and $\cos 2x$ take the same values at the 8 points. Right: the error of the kept coefficients ($|k| \leq N = 10$) of u^2 and u^3 computed on M points, against M.

17 From the plane to the sphere

On the sphere a Fourier series in longitude is natural (it is periodic), but not in latitude: the sphere is not periodic in latitude, and a latitude–longitude grid crowds its points near the poles. The natural functions are the **spherical harmonics**

$$Y_n^m(\lambda, \mu) = P_n^m(\mu)\, e^{im\lambda}, \qquad \mu = \sin\varphi, \qquad 0 \leq |m| \leq n,$$

a Fourier wave in longitude λ (zonal wavenumber m) times an associated Legendre function of latitude φ (n is the total wavenumber). We normalize so that $\frac{1}{2}\int_{-1}^{1} (P_n^m)^2\, d\mu = 1$; then the Y_n^m are orthonormal for the average over the sphere. The sign convention is the one of the ECMWF model: $P_n^m \geq 0$ near the north pole for $m \geq 0$, without the factor $(-1)^m$ (Condon–Shortley

phase) of many textbooks, and $P_n^{-m} = P_n^m$ (Ehrendorfer 2012, App. B.1 and B.3 (footnote 164: the sign is chosen "to conform with the sign convention used at ECMWF"); ECMWF 2026, Sect. 2.2.4). Durran writes $Y_{m,n}$, with the order first, for the same functions with another normalisation (Durran 2010, Sect. 6.4). The real part of Y_n^m has $n - |m|$ nodal circles of latitude and $|m|$ nodal great circles through the poles: n nodal lines in all (Figure 18). Harmonics with $m = 0$ are called zonal, with $|m| = n$ sectoral, the others tesseral. They are smooth everywhere, poles included.

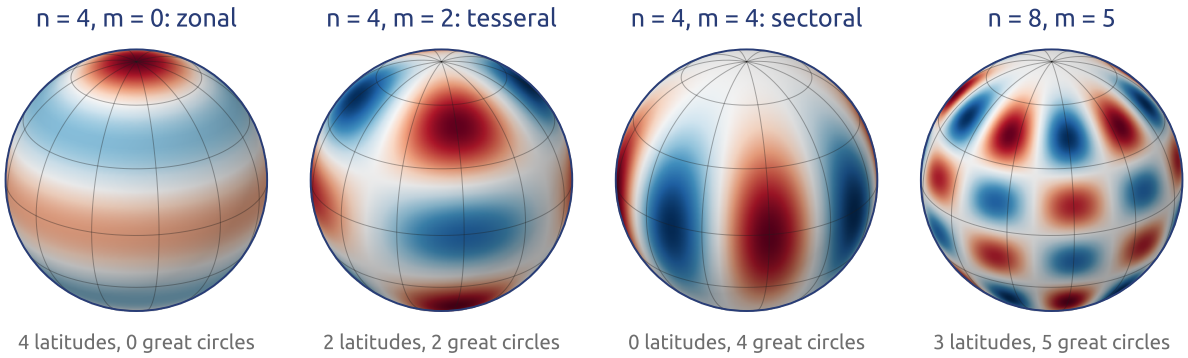


Figure 18: Spherical harmonics $P_n^m(\sin\varphi)\cos m\lambda$ seen from above 25°N: three of total wavenumber $n = 4$ (zonal, $m = 0$; tesseral, $m = 2$; sectoral, $m = 4$) and one with $n = 8$, $m = 5$. Red positive, blue negative; the colour changes on the $n - m$ nodal latitudes and the m nodal great circles. The three harmonics with $n = 4$ have the same Laplacian eigenvalue, $-20/a^2$.

18 On the sphere (1/3): the Poisson problem

The barotropic vorticity equation on the rotating sphere is

$$\frac{\partial \zeta}{\partial t} + \mathbf{u}\cdot\nabla(\zeta + f) = 0, \qquad \zeta = \nabla^2\psi, \qquad u = -\frac{1}{a}\frac{\partial\psi}{\partial\varphi}, \quad v = \frac{1}{a\cos\varphi}\frac{\partial\psi}{\partial\lambda},$$

with $f = 2\Omega\sin\varphi = 2\Omega\mu$ and a the radius of the Earth; in the plane, $\mathbf{u}\cdot\nabla q = J(\psi, q) = \psi_x q_y - \psi_y q_x$, and on the sphere $\mathbf{u}\cdot\nabla q = [\psi_\lambda q_\varphi - \psi_\varphi q_\lambda]/(a^2\cos\varphi)$. The Laplacian in $\zeta = \nabla^2\psi$ is the **spherical** Laplacian; in longitude λ and latitude φ (Vallis 2017),

$$\nabla^2 f = \frac{1}{a^2\cos\varphi}\frac{\partial}{\partial\varphi}\Big(\cos\varphi\,\frac{\partial f}{\partial\varphi}\Big) + \frac{1}{a^2\cos^2\varphi}\frac{\partial^2 f}{\partial\lambda^2}.$$

Spherical harmonics are its eigenfunctions: in the coordinates (λ, μ), with $\mu = \sin\varphi$,

$$\nabla^2 f = \frac{1}{a^2}\left[\frac{\partial}{\partial\mu}\Big((1-\mu^2)\frac{\partial f}{\partial\mu}\Big) + \frac{1}{1-\mu^2}\frac{\partial^2 f}{\partial\lambda^2}\right],$$

and P_n^m solves the associated Legendre equation $\frac{d}{d\mu}\big[(1-\mu^2)\frac{dP}{d\mu}\big] - \frac{m^2}{1-\mu^2}P = -n(n+1)P$, so that

$$\nabla^2 Y_n^m = -\frac{n(n+1)}{a^2}\,Y_n^m, \qquad \psi_n^m = -\frac{a^2}{n(n+1)}\,\zeta_n^m \qquad (n \geq 1),$$

with ψ_0^0 arbitrary (set to zero). The eigenvalue depends on n only: n sets the scale (a wavelength of about $2\pi a/n$: about 950 km for T42, 31 km for T1279), m only the orientation. The 1950 Poisson problem is a division, as with von Neumann's sines (Ehrendorfer 2012, Sect. 7.14; ECMWF 2026, Sect. 2.2.4). Expand $\zeta = \sum_{n=0}^{N}\sum_{m=-n}^{n}\zeta_n^m Y_n^m$; with the sign convention above, for a real field, $\zeta_n^{-m} = (\zeta_n^m)^*$ (with the Condon–Shortley phase it would be $(-1)^m(\zeta_n^m)^*$ (Ehrendorfer 2012, eq. 7.157; Durran 2010, eq. 6.49)), and only $m \geq 0$ is stored (Figure 19).

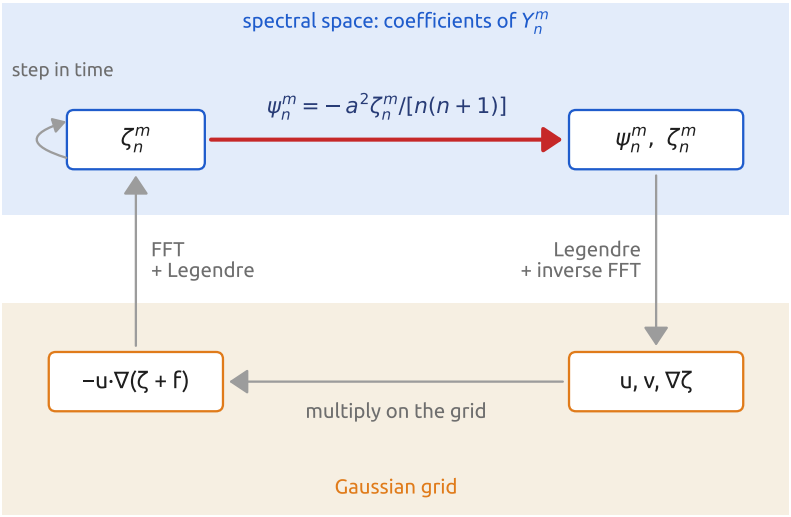


Figure 19: One time step, first part: in spectral space the Poisson problem is a division of each coefficient by $-n(n+1)/a^2$.

19 On the sphere (2/3): to the grid and back

The velocity looks singular at the poles in (u, v), but $U = u\cos\varphi$ and $V = v\cos\varphi$ are smooth:

$$U = -\frac{1}{a}(1-\mu^2)\frac{\partial\psi}{\partial\mu}, \qquad V = \frac{1}{a}\frac{\partial\psi}{\partial\lambda}.$$

The λ derivative multiplies each coefficient by im. The μ derivative uses the recursion

$$(1-\mu^2)\frac{dP_n^m}{d\mu} = -n\,\varepsilon_{n+1}^m P_{n+1}^m + (n+1)\,\varepsilon_n^m P_{n-1}^m, \qquad \varepsilon_n^m = \sqrt{\frac{n^2-m^2}{4n^2-1}},$$

so U, V, $\partial\zeta/\partial\lambda$ and $\cos\varphi\,\partial\zeta/\partial\varphi$ are computed exactly on the grid by *inverse transforms*: for each m, a sum over n (the inverse Legendre transform) at each latitude, then an inverse FFT along each latitude circle. The *direct transform* goes back: an FFT along each latitude circle gives $X_m(\mu) = \frac{1}{2\pi}\int_0^{2\pi} X\, e^{-im\lambda} d\lambda$, then a Legendre transform $X_n^m = \frac{1}{2}\int_{-1}^{1} X_m(\mu) P_n^m(\mu)\, d\mu$, computed by **Gaussian quadrature**,

$$X_n^m = \sum_{j=1}^{N_{lat}} w_j\, X_m(\mu_j)\, P_n^m(\mu_j),$$

with the Gaussian latitudes μ_j, the roots of the Legendre polynomial $P_{N_{lat}}$, and their weights w_j, normalised to sum to 1 as in the IFS documentation. The quadrature is exact for polynomials in μ of degree up to $2N_{lat}-1$ (ECMWF 2026, Sect. 2.2.4; Ehrendorfer 2012, Sect. 7.11). For the product of two fields of truncation N, the integrand is a polynomial of degree up to about $3N$, which gives the **quadratic Gaussian grid**: $N_{lat} \geq (3N+1)/2$ latitudes and $3N+1$ longitudes, the spherical form of the 2/3 rule (Figure 20).

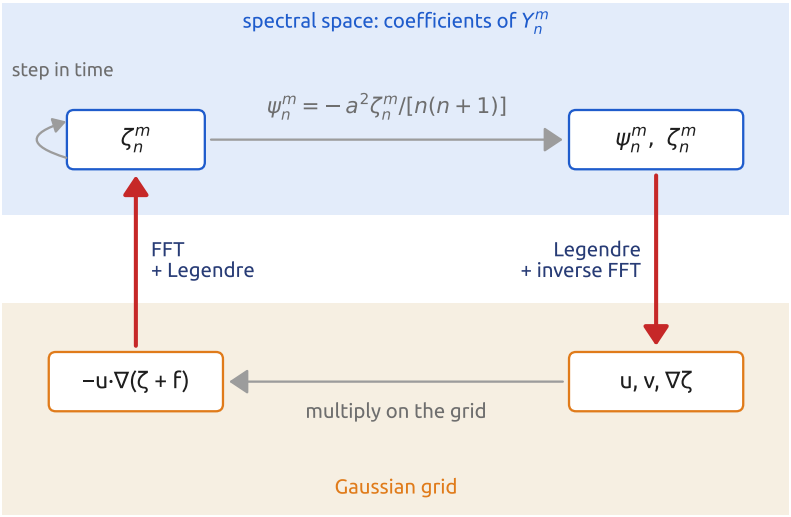


Figure 20: One time step, second part: inverse transforms (Legendre, then inverse FFT) bring u, v and $\nabla\zeta$ to the Gaussian grid; direct transforms (FFT, then Legendre by Gaussian quadrature) bring fields back.

20 On the sphere (3/3): one time step

On the grid,

$$\mathbf{u}\cdot\nabla(\zeta+f) = \frac{1}{a\cos^2\varphi}\left[U\frac{\partial\zeta}{\partial\lambda} + V\Big(\cos\varphi\frac{\partial\zeta}{\partial\varphi} + 2\Omega\cos^2\varphi\Big)\right],$$

then a direct transform gives its coefficients, and each coefficient is stepped in time:

$$\frac{d\zeta_n^m}{dt} = -\big[\mathbf{u}\cdot\nabla(\zeta+f)\big]_n^m - \nu_4\Big(\frac{n(n+1)}{a^2}\Big)^2\zeta_n^m,$$

where $[\,\cdot\,]_n^m$ is the coefficient of Y_n^m and the last term, a ∇^4 hyperdiffusion with coefficient ν_4, removes the enstrophy that cascades to the smallest scales (Ehrendorfer 2012, Sect. 7.14). Linear operators are numbers in spectral space, products are computed on the grid: the barotropic vorticity equation on the whole sphere (Figure 21). The time stepping can be leapfrog or a Runge–Kutta scheme.

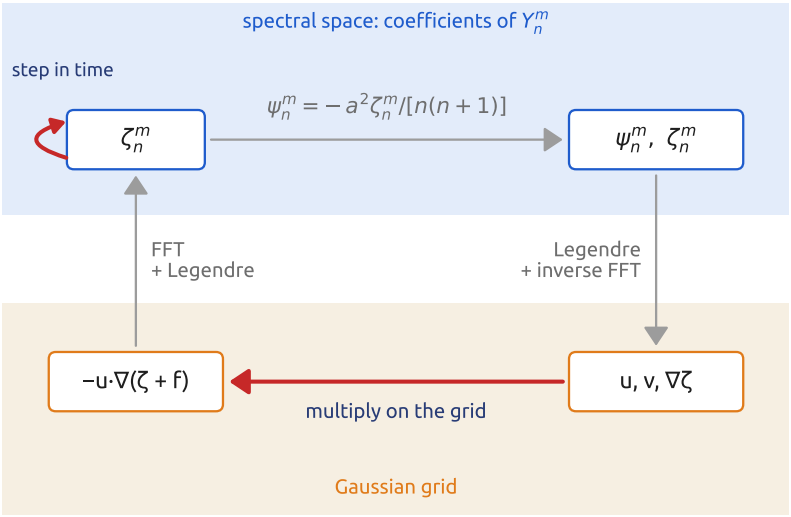


Figure 21: One time step of the barotropic vorticity equation with spherical harmonics. In spectral space (top) the Poisson problem is a division; inverse transforms give u, v and $\nabla\zeta$ on the Gaussian grid (bottom), where the product is computed; direct transforms bring it back, and each coefficient is stepped in time.

21 Triangular truncation and the Gaussian grid

Keeping all Y_n^m with $0 \le |m| \le n \le N$ is the **triangular truncation** N (the model is called TN). It is *isotropic*: the resolution is the same in every direction and at every place on the sphere. The reason is that the Laplacian commutes with rotations of the sphere, so each eigenspace (all the Y_n^m of one n, $2n+1$ functions) is mapped into itself by a rotation: rotating the sphere mixes the m of one n, never different n. A truncation that cuts at a fixed n is therefore unchanged by a rotation; a rhomboidal truncation ($|m| \le N$, $n - |m| \le N$, used in early models) is not (Ehrendorfer 2012, Sect. 7.11; Durran 2010, Sect. 6.4.1). The quadratic grid for T42 has 64 latitudes and 128 longitudes. The shortest wave of truncation TN has a wavelength of about $2\pi a/N$: about 950 km for T42. The *grid* spacing is smaller (two to four points per shortest wave), which is why the resolution of a spectral model is quoted in two ways (Figure 22). Gaussian latitudes are almost equally spaced, a little closer near the poles.

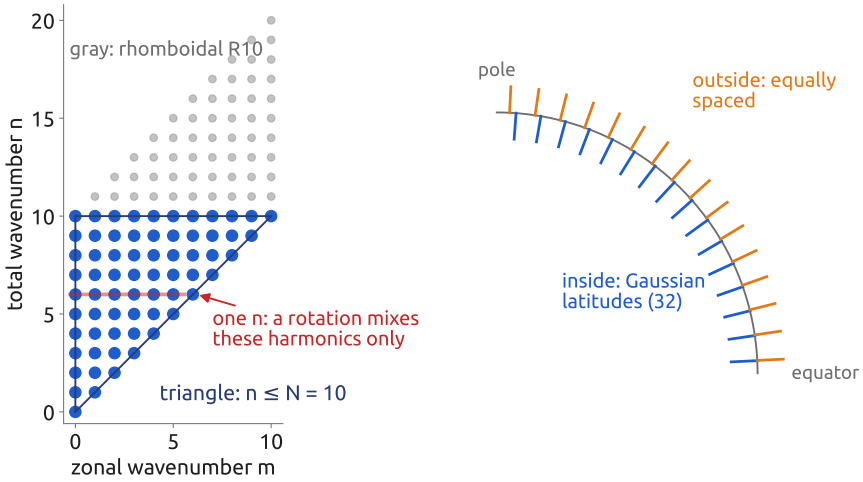


Figure 22: Left: the harmonics kept by a triangular truncation $N = 10$, $0 \le m \le n \le N$ (blue); a rotation of the sphere mixes only the harmonics of one row n. Gray: the extra harmonics of a rhomboidal truncation. Right: 32 Gaussian latitudes (inside the quarter circle) against equally spaced ones (outside).

22 In class: Rossby–Haurwitz waves

Exercise 2 — Rossby–Haurwitz waves. On the sphere, the barotropic vorticity equation linearized about rest is $\partial_t \nabla^2 \psi + (2\Omega/a^2)\,\partial_\lambda \psi = 0$. Take $\psi = A\,P_n^m(\sin\varphi)\cos(m\lambda - \sigma t)$. (a) With $\nabla^2 Y_n^m = -n(n+1)Y_n^m/a^2$, find σ and the angular speed σ/m of the pattern. East or west? (b) How many days does it take to go once round the Earth for $n = 1, 2, 5$? What is special about $n = 1$?

(c) To hand in: a stationary wave. Add an eastward wind in solid-body rotation, $u = \omega a \cos\varphi$ (the air turns a little faster than the Earth). The pattern then turns at $\omega - 2(\Omega + \omega)/[n(n+1)]$. Which ω makes the wave $n = 5$ stationary? What is u at the equator and at 45°N?

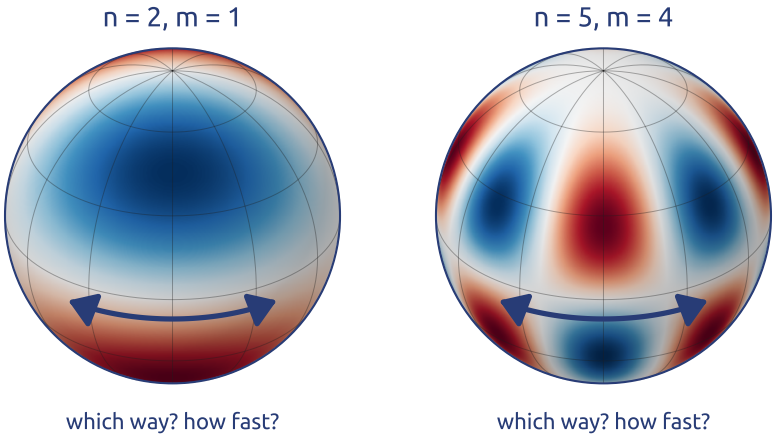


Figure 23: Two Rossby–Haurwitz patterns, $n = 2$, $m = 1$ and $n = 5$, $m = 4$, seen from above: which way do they turn, and how fast?

23 What the exercise showed

(a) With $\psi = AP_n^m \cos(m\lambda - \sigma t)$, $\partial_t \nabla^2 \psi = -\frac{n(n+1)}{a^2}\sigma A P_n^m \sin(m\lambda - \sigma t)$ and $\frac{2\Omega}{a^2}\partial_\lambda \psi = -\frac{2\Omega}{a^2} m A P_n^m \sin(m\lambda - \sigma t)$. Their sum vanishes if $\sigma = -2\Omega m/[n(n+1)]$: the pattern turns at the angular speed $\sigma/m = -2\Omega/[n(n+1)]$, westward, and the speed depends on n only (Haurwitz 1940): the largest scales are the fastest. (b) Once round the Earth in $\pi n(n+1)/\Omega$: 0.997 days for $n = 1$, 3.0 days for $n = 2$, 15 days for $n = 5$. For $n = 1$ the pattern turns westward once a day relative to the Earth, so it is fixed in space: a harmonic with $n = 1$, $m = 1$ is a solid-body rotation about a tilted axis, which the Earth turns under. (c) The pattern is stationary when $\omega - 2(\Omega + \omega)/[n(n+1)] = 0$, $\omega = 2\Omega/[n(n+1) - 2]$; for $n = 5$, $\omega = \Omega/14 = 5.2 \times 10^{-6}$ s^{-1}, so $u = \omega a \cos\varphi = 33$ m/s at the equator and 23 m/s at 45°N: Rossby's stationary waves (Figure 24). These Rossby–Haurwitz waves are the spherical version of the Rossby waves of the β-plane. (In the test case of Williamson et al. (1992) the wave is written with R, ω, K and an angular speed ν: their zonal wavenumber R is our m, the harmonic has $n = R + 1$, and ν is not the hyperdiffusion coefficient ν_4.)

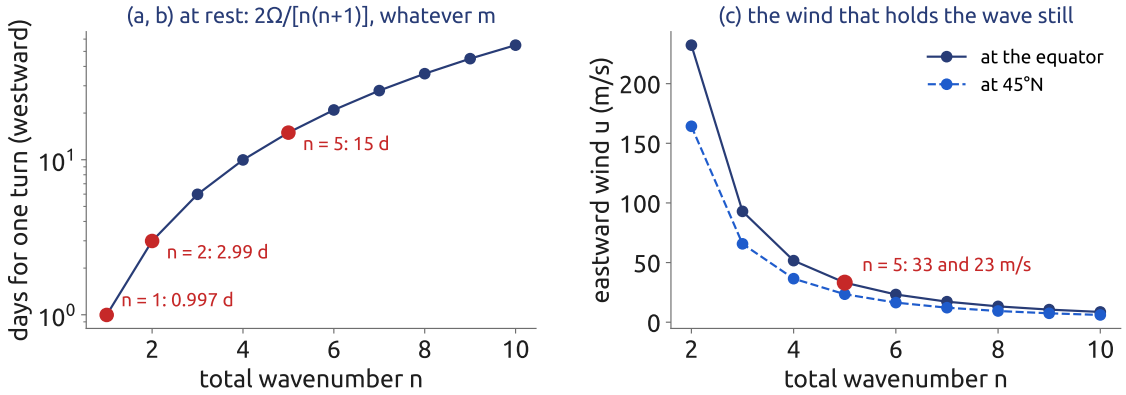


Figure 24: Left: the days a Rossby–Haurwitz pattern takes to go once round the Earth, westward, against n. Right: the eastward solid-body wind that holds the wave n still, at the equator and at 45°N.

24 The barotropic vorticity equation, computed on a plane and on the sphere

The same pseudo-spectral model of the barotropic vorticity equation runs on a doubly periodic β-plane and, with spherical harmonics, on the sphere. On the plane it reproduces the Rossby-wave frequencies $\omega = -\beta k/(k^2 + l^2)$, follows a single cyclone, and, over longer runs, two-dimensional turbulence. On the sphere it builds the transform in a few lines (Gaussian latitudes, Legendre functions by recursion, FFTs), checks the Rossby–Haurwitz waves, and runs an unstable jet (Figure 25).

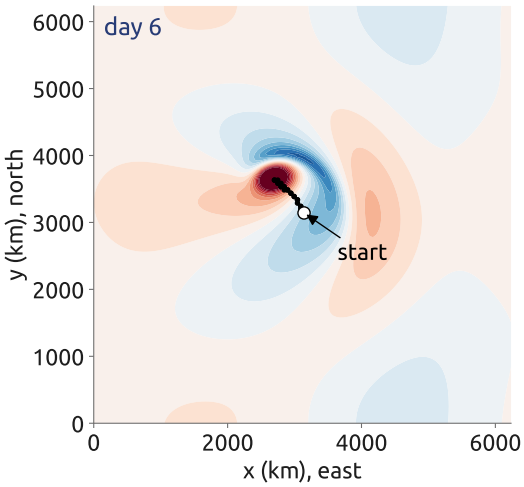


Figure 25: A cyclone on the β-plane: relative vorticity after 6 days on a 6283 km doubly periodic square (β at 45°N, 128×128 grid), with the track of the vortex centre, about 650 km north-west of its start. Colours saturated to show the Rossby-wave wake.

25 Model against exact solutions: Rossby waves, a drifting cyclone, an unstable jet

On the plane, the model's Rossby-wave frequencies equal $-\beta k/(k^2 + l^2)$ to all printed digits. The cyclone drifts **north-west** at about 1 m/s (the β drift), leaving Rossby waves behind. The Rossby–Haurwitz wave of Williamson's test case moves 122° east in 10 days with an error of 10^{-8} (only the time stepping), and at rest the waves move westward at $2\Omega/[n(n+1)]$. The unstable jet, of the shape of Galewsky et al. (2004), grows from a tiny bump into breaking waves in 4–6 days; T42 and T63 disagree by day 6 (Figure 26). On a laptop a forecast day takes seconds; on the ENIAC it took a day. A spectral model of the barotropic vorticity equation on the whole sphere fits in about sixty lines of numpy.

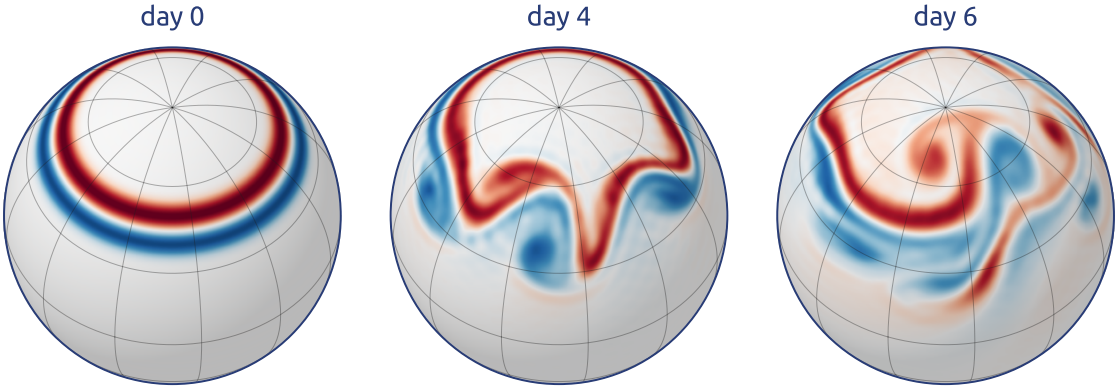


Figure 26: A barotropically unstable jet on the sphere: relative vorticity at days 0, 4 and 6, seen from above 50°N, red positive. An 80 m/s jet at 45°N with a small vorticity bump; T63 on a 95×190 Gaussian grid, RK4 with 20-minute steps and a ∇^4 hyperdiffusion.

26 Semi-implicit (1/2): the gravity-wave limit

The barotropic vorticity equation has no gravity waves. The shallow water and primitive equations do: external gravity waves move at $\sqrt{gH} \approx 300$ m/s, ten times faster than the wind, and with an explicit scheme they set the time step through the CFL condition, although they carry little energy. Take the linear shallow water equations without rotation, $\partial_t \mathbf{u} = -g\nabla\eta$, $\partial_t \eta = -H\nabla\cdot\mathbf{u}$, with η the height perturbation and H the mean depth. The divergence of the first, with $\delta = \nabla\cdot\mathbf{u}$, gives the pair

$$\frac{\partial \delta}{\partial t} = -g\nabla^2\eta, \qquad \frac{\partial \eta}{\partial t} = -H\delta,$$

and eliminating η, $\partial_{tt}\delta = gH\nabla^2\delta$: gravity waves at the speed $\sqrt{gH}$. Robert's **semi-implicit** scheme treats the linear terms that make gravity waves implicitly, as averages of the values at $t-\Delta t$ and $t+\Delta t$, and the rest explicitly (Staniforth 1997; Durran 2010, Sect. 8.2). For an oscillation $dF/dt = i\omega F$, leapfrog is stable only for $\omega\Delta t \le 1$, with $\sin(\omega_{\text{num}}\Delta t) = \omega\Delta t$, while the averaged treatment gives $\tan(\omega_{\text{num}}\Delta t) = \omega\Delta t$, stable for every Δt: slow waves are accurate, fast gravity waves are slowed down but harmless (Figure 27). Robert's idea started, Staniforth tells, at a seminar on implicit methods by G. I. Marchuk.

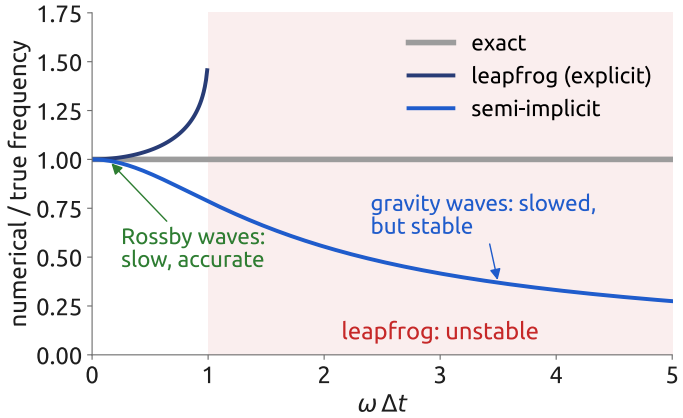


Figure 27: Numerical frequency against $\omega\Delta t$ for the oscillation equation: exact, leapfrog (unstable beyond $\omega\Delta t = 1$) and the semi-implicit average (stable, the fast waves slowed).

27 Semi-implicit (2/2): Helmholtz, a division

With the other terms (nonlinear, Coriolis) collected in R_δ and R_h and treated explicitly, the leapfrog step with the linear terms averaged is (with $\pm$ for the time levels $t \pm \Delta t$, to keep n for the total wavenumber)

$$\delta^+ = \delta^- - g\Delta t\,\nabla^2(\eta^+ + \eta^-) + 2\Delta t R_\delta, \qquad \eta^+ = \eta^- - H\Delta t\,(\delta^+ + \delta^-) + 2\Delta t R_h.$$

Eliminating η^+ gives a Helmholtz equation for δ^+,

$$(1 - gH\Delta t^2\,\nabla^2)\,\delta^+ = R,$$

with R everything known at t and $t-\Delta t$; in spherical harmonics it is again a division: $\delta_n^{m,+} = R_n^m/[1 + gH\Delta t^2\, n(n+1)/a^2]$. "This is negligible for a spectral model", as Staniforth writes of the cost of the Helmholtz problem (Staniforth 1997, 35). A grid-point model must instead solve an elliptic problem on the whole globe at every step, usually by an iterative method. In a model

with many levels, the gravity-wave terms couple the levels through the hydrostatic relation, and the Helmholtz problem becomes, for each (m, n), a small linear system $\left[I + \frac{n(n+1)}{a^2}\Gamma\right] D_n^{m,+} = \tilde{D}_n^m$ for the divergence at all levels at $t + \Delta t$, where Γ is a matrix of the size of the number of levels (ECMWF 2026, Sect. 2.2.7, Eq. 2.50; Durran 2010, Sect. 8.2.3). Its eigenvectors are vertical normal modes, and its eigenvalues, $gh_k\Delta t^2$ up to a constant factor, give their equivalent depths h_k: in the basis of the modes the system splits into one Helmholtz problem, and one division, per mode.

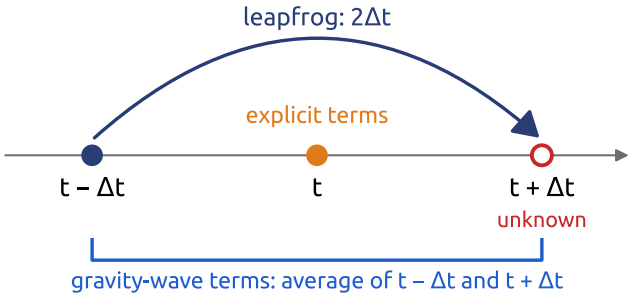


Figure 28: The semi-implicit leapfrog step in time: leapfrog jumps from $t - \Delta t$ over t to $t + \Delta t$; the explicit terms (advection, Coriolis) are evaluated at t; the gravity-wave terms are the average of $t - \Delta t$ and $t + \Delta t$, so they involve the unknown at $t + \Delta t$: a Helmholtz problem for it.

28 The grids of the IFS

Near the poles a harmonic of large m is tiny, so fewer points per latitude circle are needed there: the Gaussian grid of the ECMWF model is *reduced* towards the poles since 1991 (Hortal and Simmons 1991). Since March 2016 the grid is *octahedral*: 20 points on the latitude next to each pole and 4 more on each latitude towards the equator (ECMWF 2026, Sect. 2.2.5; Malardel et al. 2016). For 1280 latitudes per hemisphere this gives $2\sum_{i=1}^{1280}(20 + 4(i-1)) = 6\,599\,680$ points per level, against about 8.5 million for the earlier reduced grid: 22% cheaper. The grid paired with truncation N has 2, 3 or 4 points per shortest wave (linear, quadratic, cubic). The quadratic grid (the 2/3 rule) was used until 1998; the semi-Lagrangian scheme allowed the cheaper linear grid; at high resolution aliasing came back, and in 2016 ECMWF moved to the *cubic* grid, which has almost no aliasing: TCo1279 is truncation 1279 on the cubic octahedral grid with 1280 latitudes per hemisphere, about 9 km (ECMWF 2026, Sect. 2.2.6; Malardel et al. 2016) (Figure 29). A spectral model can drop points near the poles because the truncation already removes the short waves there; a latitude–longitude finite-difference model cannot.

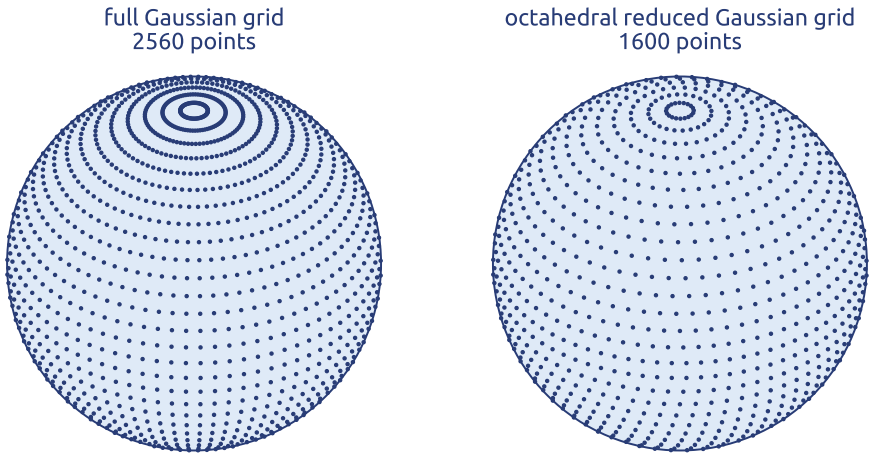


Figure 29: Two Gaussian grids with 16 latitudes per hemisphere and 80 points on the latitudes next to the equator, seen from above 35°N. Left: the full grid, 80 points on every latitude, crowded at the poles (2560 points). Right: the octahedral reduced grid of the IFS, 20 points next to each pole and 4 more per latitude towards the equator (1600 points).

29 IFS today

The Integrated Forecasting System of ECMWF has been a spectral model since April 1983, when ECMWF's first spectral model went into operations (ECMWF 2026, Sect. 2.2.4). Its current cycle (Cy50r1, operational since 12 May 2026) runs the medium-range forecasts at TCo1279, a grid spacing of about 9 km, with 137 levels up to 0.01 hPa, and an ensemble of 50 members plus a control at the same resolution (ECMWF model information page, Cy50r1). The main ingredients (Figure 30):

- **Spectral transform.** The wind, the virtual temperature and the surface pressure go to spectral space and back at every time step; specific humidity, clouds and tracers stay on the grid, since transforms can create negative values in non-smooth fields (ECMWF 2026, Sect. 2.2.4).
- **Semi-Lagrangian advection.** Instead of the Eulerian $\mathbf{u} \cdot \nabla$, each grid point looks back along the trajectory to its departure point and interpolates the field there. This is stable for long time steps.
- **Semi-implicit time stepping,** with the Helmholtz problem solved in spectral space. Together, a time step of several minutes at 9 km: 400 s in Malardel et al. (2016).

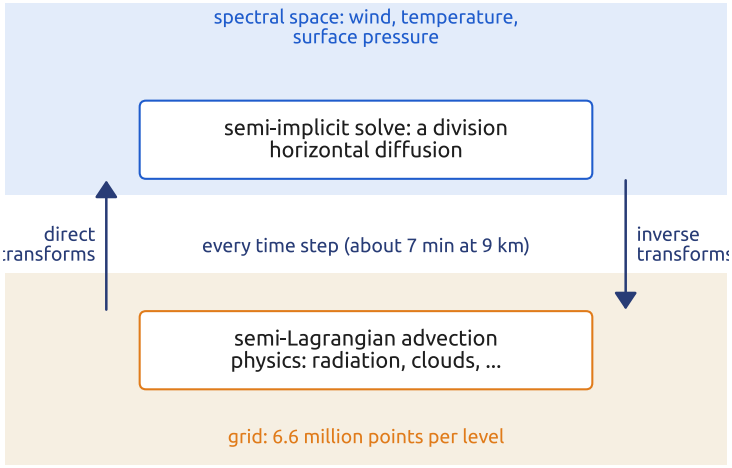


Figure 30: One time step of the IFS: the semi-implicit solve in spectral space, the semi-Lagrangian advection and the physics on the grid, and the transforms between them.

30 The cost of the transforms

For triangular truncation N on a quadratic grid there are about $N^2/2$ coefficients (m, n) with $m \geq 0$ and about $1.5\,N$ latitudes, so a Legendre transform of one field costs about $0.75\,N^3$ operations, while the FFTs cost $O(N^2 \log N)$ and the grid has $O(N^2)$ points (Williamson 2007) (Figure 31). Doubling the resolution multiplies the grid by 4, the Legendre work by 8, and halves the time step. Fast Legendre transforms that exploit the structure of the P_n^m reduce this cost substantially at high resolution (Wedi et al. 2013). The harder problem is communication: every coefficient depends on every grid point, so each transform requires a global exchange of data ("transpositions") across the whole supercomputer, at every time step. In the words of the IFS documentation, these "remain a concern on future computing architectures" (ECMWF 2026, Sect. 2.2.4). Methods that only exchange data with neighbours, finite volumes and finite elements on quasi-uniform grids, are the alternative.

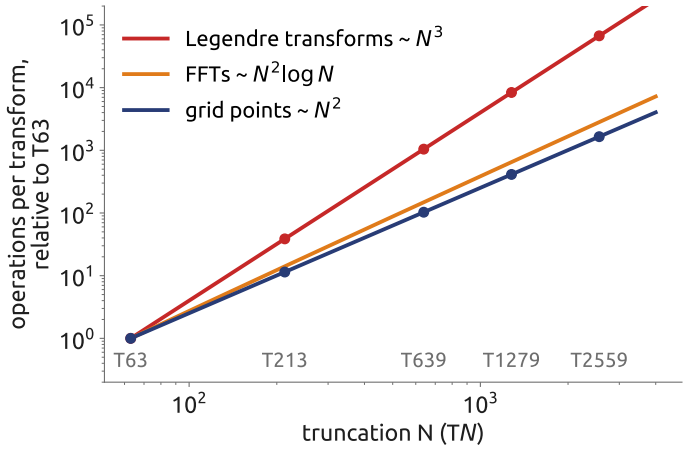


Figure 31: Operations for one transform of one field, at one time step, on a quadratic Gaussian grid (about $1.5N$ latitudes and $3N$ longitudes), against the truncation N: Legendre transforms ($0.75N^3$), FFTs ($1.5N \times 3N \log_2 3N$) and grid points ($4.5N^2$), each divided by its own value at T63. The curves show how fast each part grows, not which costs most: with these counts the Legendre transforms cost about 1.4 times the FFTs at T63 and about 18 times at T1279. Operation counts only: no fast Legendre transform, no communication, and the shorter time step of a finer grid not included.

31 Spectral models today

Spectral models are not a thing of the past (Figure 32). Besides the IFS, Météo-France's global model ARPEGE is spectral on a *stretched* sphere: a conformal (Schmidt) transformation moves the pole of the harmonics over France and concentrates the resolution there (Courtier and Geleyn 1988); in 2016 it ran at T1198 with a stretching factor 2.2, from about 7 km over France to 33 km over the South Pacific. Its limited-area relatives ALADIN and AROME are spectral on a plane: a Fourier series in x and y (bi-Fourier), made periodic by an extension zone added to the domain; AROME-France runs at 1.3 km (Météo-France 2016; Seity et al. 2011). The Global Spectral Model of the Japan Meteorological Agency (GSM) moved in March 2023 from a linear to a quadratic grid, TQ959, about 13 km, to reduce the small-scale noise of spectral blocking (Yonehara et al. 2025). In climate, the European Earth system model EC-Earth3 couples the IFS (the atmosphere and land, at T255 with 91 levels, about 80 km) to the ocean model NEMO and its sea ice; it is built by a consortium of 27 partners in ten European countries, in Italy the Institute of Atmospheric Sciences and Climate of the National Research Council (ISAC-CNR, Bologna and Turin), the energy agency ENEA (Rome) and the Politecnico di Torino (Döscher et al. 2022). The Brazilian Global Atmospheric Model of CPTEC (BAM) is a spectral, semi-implicit model (Eulerian or semi-Lagrangian), run at TQ0666, about 20 km (Figueroa et al. 2016); the High-Resolution Global Forecast Model of IITM, India (HGFM, the basis of the Bharat Forecast System), uses the cubic octahedral grid at TCo1534, about 6.5 km in the tropics (Krishna et al. 2025); China's YHGSM (National University of Defense Technology) is a spectral model with semi-Lagrangian advection (Jiang et al. 2021). The United States went spectral first: the global spectral model of the National Meteorological Center (now NCEP) became operational in August 1980 (Sela 1980), three years before ECMWF's; run as the AVN and MRF forecasts, it was renamed the Global Forecast System (GFS) in 2002, and it stayed spectral until June 2019, when it moved to the finite-volume cubed-sphere core FV3 (NCEP, GFS documentation). ECMWF also develops a finite-volume core (FVM) for the future.

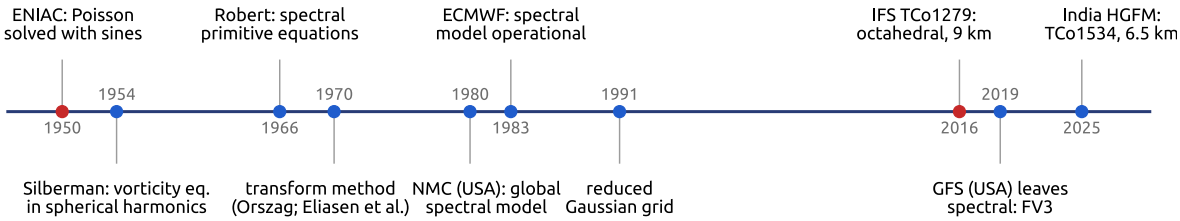


Figure 32: A timeline of spectral models: from von Neumann's sines (1950) and Silberman's spherical harmonics (1954) to the transform method (1970), ECMWF's spectral model (1983), the reduced and octahedral grids, and the models of today.

32 A Galerkin method

Following Durran (2010, Sect. 6.1), write the equation as $\partial_t u + F(u) = 0$, with F the terms with space derivatives, and truncate the field to the kept waves, $u_N = \sum_{|k|\le N} \hat{u}_k\, e^{ikx}$. The truncated field cannot satisfy the equation exactly: the product in F makes waves up to $2N$ (Figure 33, left). What is left is the *residual* $R = \partial_t u_N + F(u_N)$. The **Galerkin approximation** asks the residual to be orthogonal to every expansion function kept,

$$\int_0^{2\pi} R\, e^{-ikx}\, dx = 0 \qquad \text{for every } |k| \le N,$$

which gives one ordinary differential equation per kept coefficient: $d\hat{u}_k/dt$ is minus the coefficient k of $F(u_N)$. This is the spectral method, and the transform method computes it exactly when the products are not aliased (the 2/3 rule): the waves of the product beyond N, the residual, are dropped.

The Galerkin condition conserves what the equation conserves (Durran 2010, Sect. 6.2.3). Let P_N be the orthogonal projection onto the waves $|k| \le N$. For Burgers' equation the dealiased spectral method is $\partial_t u_N = -P_N(u_N\, \partial_x u_N)$, and

$$\frac{d}{dt}\,\frac{1}{2}\int u_N^2\, dx = -\int u_N\, P_N(u_N\, \partial_x u_N)\, dx = -\int u_N^2\, \partial_x u_N\, dx = -\int \partial_x\Big(\frac{u_N^3}{3}\Big) dx = 0,$$

because P_N is self-adjoint and $P_N u_N = u_N$. The energy is conserved whatever the nonlinearity, so there is no nonlinear instability; only the time stepping can add errors. With aliasing the computed product is not $P_N(u_N\, \partial_x u_N)$ and the identity fails: on 64 points the aliased run blows up, the dealiased one keeps its energy (Figure 33, right).

Finite elements use the same Galerkin condition with other expansion functions: instead of global waves, local functions, each non-zero on a few cells of a mesh of any shape (Durran 2010, Sect. 6.5).

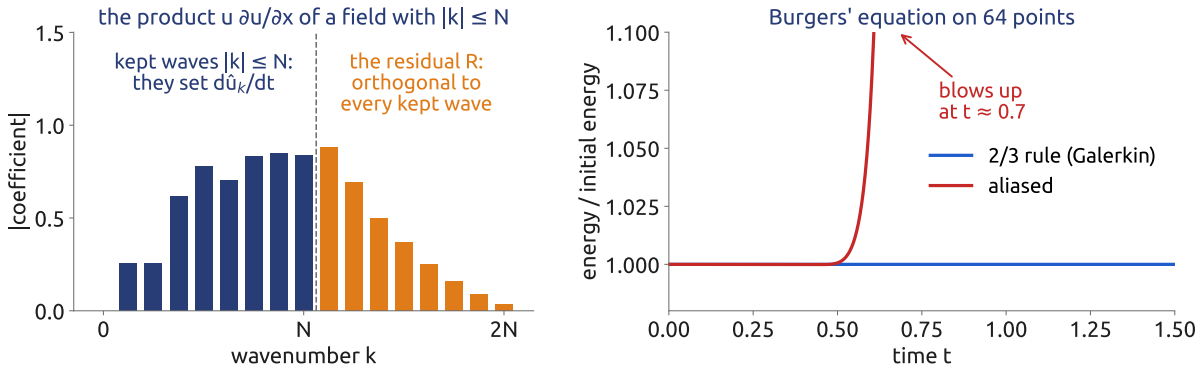


Figure 33: Left: the coefficients of $u_N\,\partial_x u_N$ for a field with the waves $1 \le k \le N = 8$: the kept ones set $d\hat{u}_k/dt$, the others form the residual, orthogonal to every kept wave. Right: the energy of the inviscid Burgers equation, $u_0 = \sin x + 0.3\sin(3x+1)$, on 64 points with RK4 ($\Delta t = 10^{-3}$), relative to its initial value: with the 2/3 rule ($N = 21$, the Galerkin method) it stays constant, also after the shock forms at $t = 0.54$; with all the grid's waves (aliased) it drifts and the run blows up at $t \approx 0.7$.

33 Key points

1. **Spectral derivative:** exact for every resolved wave; spectral accuracy for smooth fields; ringing at jumps.
2. **Transform method:** products on the grid; **aliasing**; the 2/3 rule ($3N+1$ points).
3. **Spherical harmonics** Y_n^m: $\nabla^2 Y_n^m = -n(n+1)Y_n^m/a^2$; triangular truncation N (TN); Gaussian grid; no pole problem.
4. Poisson and Helmholtz problems are divisions: **semi-implicit** steps are cheap.
5. Legendre transforms cost $\sim N^3$ and need **global communication**: the scaling limit.
6. **The IFS:** spectral, semi-Lagrangian, semi-implicit, 9 km.
7. **A Galerkin method:** the residual is orthogonal to every kept wave; energy conserved without aliasing.

Spectral methods: exact derivatives and cheap implicit steps, at the price of global transforms. Still open: jumps and positive fields such as moisture, which the IFS keeps on the grid; and the global communication, which the Galerkin idea with *local* basis functions on any mesh, the finite elements, avoids.

Further reading

Durran (2010), Chapter 6 (spectral, pseudospectral, spherical harmonics) and Section 8.2 (semi-implicit); Ehrendorfer (2012), a whole book on spectral weather models, built around a small model (PEAK); Fornberg (1996) for the numerical analysis of pseudospectral methods; Williamson (2007) for the history of dynamical cores; ECMWF (2026) for the IFS; Lynch (2008) and Platzman (1979) for the 1950 forecast and von Neumann's solver.

References

Charney, Jule G., Ragnar Fjørtoft, and John von Neumann. 1950. "Numerical Integration of the Barotropic Vorticity Equation." *Tellus* 2 (4): 237–54. https://doi.org/10.3402/tellusa.v2i4.8

607.

Courtier, Philippe, and Jean-François Geleyn. 1988. "A Global Numerical Weather Prediction Model with Variable Resolution: Application to the Shallow-Water Equations." *Quarterly Journal of the Royal Meteorological Society* 114 (483): 1321–46. https://doi.org/10.1002/qj.49711448309.

Döscher, Ralf, Mario Acosta, Andrea Alessandri, et al. 2022. "The EC-Earth3 Earth System Model for the Coupled Model Intercomparison Project 6." *Geoscientific Model Development* 15 (7): 2973–3020. https://doi.org/10.5194/gmd-15-2973-2022.

Durran, Dale R. 2010. *Numerical Methods for Fluid Dynamics: With Applications to Geophysics*. 2nd ed. Vol. 32. Texts in Applied Mathematics. Springer.

ECMWF. 2026. *IFS Documentation CY50R1, Part III: Dynamics and Numerical Procedures*. European Centre for Medium-Range Weather Forecasts. https://doi.org/10.21957/b4d9609507.

Ehrendorfer, Martin. 2012. *Spectral Numerical Weather Prediction Models*. Society for Industrial; Applied Mathematics.

Eliasen, Erik, Bennert Machenhauer, and Erik Rasmussen. 1970. *On a Numerical Method for Integration of the Hydrodynamical Equations with a Spectral Representation of the Horizontal Fields*. Report No. 2. Institute of Theoretical Meteorology, University of Copenhagen.

Figueroa, Silvio N., José P. Bonatti, Paulo Y. Kubota, et al. 2016. "The Brazilian Global Atmospheric Model (BAM): Performance for Tropical Rainfall Forecasting and Sensitivity to Convective Scheme and Horizontal Resolution." *Weather and Forecasting* 31 (5): 1547–72. https://doi.org/10.1175/WAF-D-16-0062.1.

Fornberg, Bengt. 1996. *A Practical Guide to Pseudospectral Methods*. Cambridge Monographs on Applied and Computational Mathematics. Cambridge University Press.

Galewsky, Joseph, Richard K. Scott, and Lorenzo M. Polvani. 2004. "An Initial-Value Problem for Testing Numerical Models of the Global Shallow-Water Equations." *Tellus A* 56 (5): 429–40. https://doi.org/10.3402/tellusa.v56i5.14436.

Haurwitz, Bernhard. 1940. "The Motion of Atmospheric Disturbances on the Spherical Earth." *Journal of Marine Research* 3 (3). https://elischolar.library.yale.edu/journal_of_marine_research/575.

Hortal, Mariano, and Adrian J. Simmons. 1991. "Use of Reduced Gaussian Grids in Spectral Models." *Monthly Weather Review* 119 (4): 1057–74. https://doi.org/10.1175/1520-0493(1991)119%3C1057:UORGGI%3E2.0.CO;2.

Jiang, Tao, Jianping Wu, Zhaoyang Liu, Wenpeng Zhao, and Yongshun Zhang. 2021. "Optimization of the Parallel Semi-Lagrangian Scheme Based on Overlapping Communication with Computation in the YHGSM." *Quarterly Journal of the Royal Meteorological Society* 147: 2293–302. https://doi.org/10.1002/qj.4023.

Krishna, R. Phani Murali, Siddharth Kumar, A. G. Prajeesh, Peter Bechtold, Nils Wedi, et al.

2025. “Indian Institute of Tropical Meteorology (IITM) High-Resolution Global Forecast Model Version 1: An Attempt to Resolve Monsoon Prediction Deadlock.” *Geoscientific Model Development* 18: 1879–94. https://doi.org/10.5194/gmd-18-1879-2025.

Lynch, Peter. 2008. “The ENIAC Forecasts: A Re-Creation.” *Bulletin of the American Meteorological Society* 89 (1): 45–55. https://doi.org/10.1175/BAMS-89-1-45.

Malardel, Sylvie, Nils Wedi, Willem Deconinck, et al. 2016. “A New Grid for the IFS.” *ECMWF Newsletter*, no. 146: 23–28. https://doi.org/10.21957/zwdu9u5i.

Météo-France. 2016. *The Météo-France Operational NWP System: Description and Recent Changes (May 2016)*. CNRM, Météo-France. https://cnrm.sedoo.fr/nwpreport_2016-3/.

Orszag, Steven A. 1970. “Transform Method for the Calculation of Vector-Coupled Sums: Application to the Spectral Form of the Vorticity Equation.” *Journal of the Atmospheric Sciences* 27 (6): 890–95. https://doi.org/10.1175/1520-0469(1970)027%3C0890:TMFTCO%3E2.0.CO;2.

Orszag, Steven A. 1971. “On the Elimination of Aliasing in Finite-Difference Schemes by Filtering High-Wavenumber Components.” *Journal of the Atmospheric Sciences* 28 (6): 1074. https://doi.org/10.1175/1520-0469(1971)028%3C1074:OTEOAI%3E2.0.CO;2.

Platzman, George W. 1979. “The ENIAC Computations of 1950: Gateway to Numerical Weather Prediction.” *Bulletin of the American Meteorological Society* 60 (4): 302–12. https://doi.org/10.1175/1520-0477(1979)060%3C0302:TECOTN%3E2.0.CO;2.

Robert, André J. 1966. “The Integration of a Low Order Spectral Form of the Primitive Meteorological Equations.” *Journal of the Meteorological Society of Japan* 44 (5): 237–45. https://doi.org/10.2151/jmsj1965.44.5_237.

Seity, Y., P. Brousseau, S. Malardel, et al. 2011. “The AROME-France Convective-Scale Operational Model.” *Monthly Weather Review* 139 (3): 976–91. https://doi.org/10.1175/2010MWR3425.1.

Sela, Joseph G. 1980. “Spectral Modeling at the National Meteorological Center.” *Monthly Weather Review* 108 (9): 1279–92. https://doi.org/10.1175/1520-0493(1980)108%3C1279:SMATNM%3E2.0.CO;2.

Silberman, Isadore. 1954. “Planetary Waves in the Atmosphere.” *Journal of Meteorology* 11 (1): 27–34. https://doi.org/10.1175/1520-0469(1954)011%3C0027:PWITA%3E2.0.CO;2.

Staniforth, Andrew. 1997. “André Robert (1929–1993): His Pioneering Contributions to Numerical Modelling.” *Atmosphere-Ocean* 35 (sup1): 25–54. https://doi.org/10.1080/07055900.1997.9687341.

Vallis, Geoffrey K. 2017. *Atmospheric and Oceanic Fluid Dynamics: Fundamentals and Large-Scale Circulation*. 2nd ed. Cambridge University Press. https://doi.org/10.1017/9781107588417.

Wedi, Nils P., Mats Hamrud, and George Mozdzynski. 2013. “A Fast Spherical Harmonics Transform for Global NWP and Climate Models.” *Monthly Weather Review* 141 (10): 3450–61.

https://doi.org/10.1175/MWR-D-13-00016.1.

Williamson, David L. 2007. "The Evolution of Dynamical Cores for Global Atmospheric Models." *Journal of the Meteorological Society of Japan* 85B: 241–69. https://doi.org/10.2151/jmsj.85B.241.

Williamson, David L., John B. Drake, James J. Hack, Rüdiger Jakob, and Paul N. Swarztrauber. 1992. "A Standard Test Set for Numerical Approximations to the Shallow Water Equations in Spherical Geometry." *Journal of Computational Physics* 102 (1): 211–24. https://doi.org/10.1016/S0021-9991(05)80016-6.

Yonehara, Hitoshi, Yukihiro Kuroki, Masashi Ujiie, Chihiro Matsukawa, Takafumi Kanehama, et al. 2025. *Upgrade of JMA's Operational Global Numerical Weather Prediction System*. Technical Review No. 27. Japan Meteorological Agency, RSMC Tokyo – Typhoon Center. https://www.jma.go.jp/jma/jma-eng/jma-center/rsmc-hp-pub-eg/techrev/text27-1.pdf.